Fingering instability of thin evaporating liquid films

A. V. Lyushnin,[1] A. A. Golovin,[2] and L. M. Pismen[1,3]
[1]*Department of Chemical Engineering, Technion–Israel Institute of Technology, Haifa 32000, Israel*
[2]*Department of Engineering Sciences and Applied Mathematics, Northwestern University, Evanston, Illinois 60208-3100*
[3]*Minerva Center for Nonlinear Physics of Complex Systems, Technion–Israel Institute of Technology, Haifa 32000, Israel*
(Received 8 June 2001; published 3 January 2002)

The fingering instability of growing dry patches in an evaporating film of a polar liquid placed on a solid substrate is investigated. The instability manifests itself as fingering of mobile fronts between growing ''dry'' (thin) and shrinking ''wet'' (thick) regions of the film corresponding to two stable states of the evaporating film in contact with its vapor. The boundaries of the fingering instability are found through linear stability analysis of numerical solutions of the nonlinear evolution equation defining the film profile, and the influence of the evaporation rate, polar intermolecular forces, and chemical heterogeneity of the substrate is investigated.

DOI: 10.1103/PhysRevE.65.021602 PACS number(s): 68.15.+e, 47.20.Ma, 47.54.+r, 68.08.−p

I. INTRODUCTION

The fingering instability of a moving gas-liquid-solid contact line, driven by gravity or thermocapillarity, has been observed experimentally and studied theoretically in a number of investigations [1–6]. The contact line region is usually formed by a sharp moving front between two domains—a ''thick'' bulk film and a ''thin'' precursor film. The contact line instability is caused by the formation of a ridge on this front which becomes unstable due to a mechanism analogous to the Rayleigh instability of a liquid cylinder. The instability results in the development of ''fingers''—liquid rivulets protruding toward the dry region.

A similar phenomenon is also observed during drying out of thin films of polar fluids (water) [7–9] as well as during dewetting of polymer solutions [10]. In the course of evaporation of a film of a polar liquid, nucleation of circular ''dry'' spots is observed, which are claimed to be regions covered by a very thin residual film [8,9]. These ''dry'' regions grow in size until after some time they become unstable with respect to corrugations of the moving boundary between the thin residual film and the thick initial film.[1] The aim of this article is to investigate this instability, which has not been explained so far.

A characteristic feature of polar fluids is the presence of both long-range van der Waals intermolecular forces and short-range polar forces associated with the electrical double layer. Due to the presence of the polar intermolecular forces, the dependence of the film free energy g on the film thickness h can acquire a double-well shape (see [8] for details). The dependence of the film chemical potential $\mu = dg/dh$ on h becomes nonmonotonic, as shown in Fig. 1. In this case, if a film is in equilibrium with its vapor, there can be two stable equilibrium values of the film thickness h_1 and h_2, and one unstable value in between. A film whose thickness h is between h_1 and h_2 undergoes ''spinodal decomposition'' into two stable states [8,11,12].

Consider a film of a polar fluid which is in equilibrium with its vapor and has an equilibrium thickness h_2. If the vapor pressure is gradually reduced, this causes the film evaporation and the equilibrium thickness h_2 decreases. Beyond the point of Maxwell construction the ''thick'' state becomes metastable, and fluctuations may cause nucleation of the other stable state, with a smaller thickness h_1 and lower free energy. The probability of nucleation grows when h_2 approaches the minimum point of the dependence dg/dh (see Fig. 1). This state, a ''dry spot,'' will propagate into the thicker state, exhibiting ''dry spot'' growth. In the following, we do not consider the nucleation stage, which depends on the level of noise in the system, but investigate the stage of steady growth of dry spots described by a propagating front dividing the thin (''dry'') and thick (''wet'') regions. Under certain conditions, the propagating front between the two states becomes unstable and exhibits fingering. This fits qualitatively the observations of Samid-Merzel *et al.* [8,9]. Below we investigate the conditions for this instability to occur.

II. GOVERNING EQUATION

Consider a thin layer of a polar liquid (e.g., water) of thickness h, placed horizontally between a solid substrate

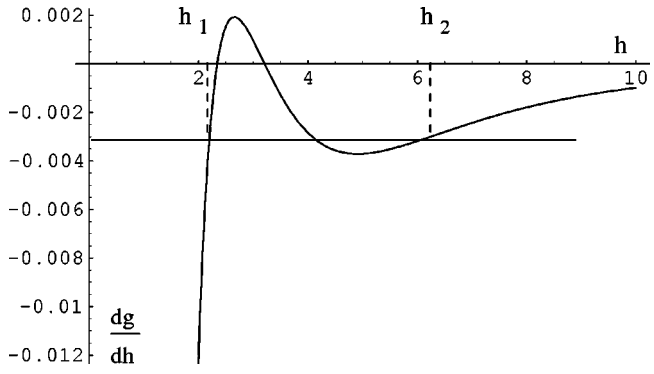

FIG. 1. A nonmonotonic chemical potential resulting from combined action of polar and van der Waals forces as a function of film thickness h. The dashed lines mark the two alternative values of the stable equilibrium thickness.

[1]This boundary is actually a narrow region where the film thickness changes sharply.

and the vapor of the same liquid. The liquid can evaporate from the film into the vapor phase.

The film evolution is described by the following equation [12,13]:

$$\frac{\partial h}{\partial t}=\nabla\cdot\frac{h^3}{3\eta}\nabla\left[\frac{dg(h)}{dh}-\gamma\nabla^2 h\right]-\frac{\epsilon}{\rho}\left[\frac{dg(h)}{dh}-\gamma\nabla^2 h-\rho\mu_v\right], \tag{1}$$

where η is the liquid viscosity, γ is the liquid-vapor surface tension, ρ is the liquid density, μ_v is the vapor chemical potential, ϵ is the parameter characterizing the evaporation rate (which can be either obtained from the gas kinetic theory or found experimentally), and

$$g(h)=\frac{S^{\mathrm{LW}}d_0^2}{h^2}+S^P\exp\frac{d_0-h}{l_0} \tag{2}$$

is the free energy due to intermolecular interactions [12], $S^{\mathrm{LW}}d_0^2=-A/(12\pi)$, A is the Hamaker constant, d_0 is the molecular interaction distance, and l_0 is the Debye length. For wetting polar liquids, $A<0$ and $S^P<0$.

We introduce the scaling $x\to\alpha x$, $t\to\beta t$, $h\to\delta h$, with

$$\alpha=\left(\frac{\delta\gamma}{S^{\mathrm{PN}}}\right)^{1/2},\quad \beta=\frac{3\eta\gamma}{\delta(S^{\mathrm{PN}})^2},$$

$$\delta=\left(\frac{A}{6\pi S^{\mathrm{PN}}}\right)^{1/3},\quad S^{\mathrm{PN}}=\frac{S^P}{l_0}\exp(d_0/l_0), \tag{3}$$

and rewrite Eq. (1) in the following dimensionless form:

$$h_t=\nabla\cdot\left[h^3\cdot\nabla\left(-\nabla^2 h-\frac{1}{h^3}+\exp(-\chi h)\right)\right]-\Omega\left[-\nabla^2 h-\frac{1}{h^3}+\exp(-\chi h)-M\right]. \tag{4}$$

This equation contains three dimensionless parameters:

$$\Omega=\frac{18\pi\epsilon\nu\gamma}{(6\pi A^2 S^{\mathrm{PN}})^{1/3}},\quad M=\frac{\rho\mu_v}{S^{\mathrm{PN}}},$$

$$\chi=\frac{1}{l_0}\left(\frac{|A|}{6\pi S^{\mathrm{PN}}}\right)^{1/3}, \tag{5}$$

where $\Omega>0$, $M<0$, and $\chi>0$ characterize the rate of evaporation, the vapor chemical potential, and the Debye length, respectively.

Using the typical values $A=10^{-20}$ J, $d_0=0.2$ nm, $l_0=0.6$ nm, $\eta=10^{-3}$ g/m s, $\gamma=0.08$ J/m^2, and $S^P=0.002$ J/m^2 [12] yields the values of the dimensionless parameters $\Omega=0.02$, $M=-0.003$, and $\chi=1.09$. Note that the dependence of the chemical potential $\mu=dg/dh$ of the liquid film on the film thickness h is nonmonotonic, and for some fixed values of the vapor chemical potential μ_v there are two stable equilibrium values of the film thickness h_1 and h_2 (see Fig. 1).

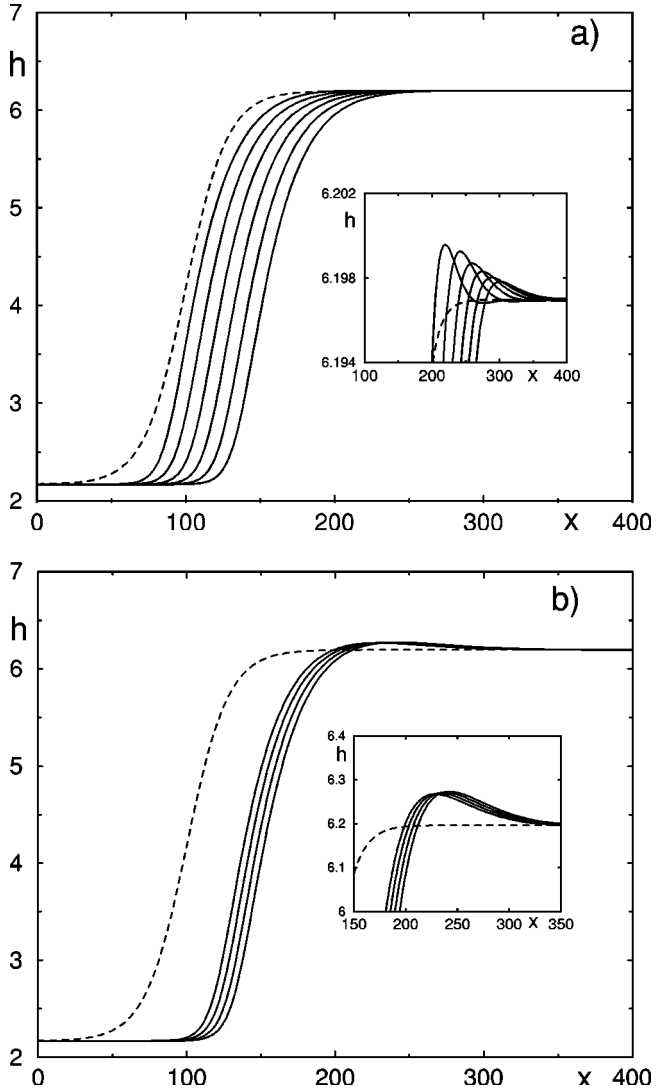

FIG. 2. Time sequences of propagating fronts for $M=-0.003$ and $\chi=1.085$, and $\Omega=0.78$ (a) and 0.078 (b). The initial profile is shown by the dashed line. The inset shows the enlargement of the bump region.

III. UNIFORMLY PROPAGATING FRONTS

Equation (4) has been solved numerically by means of a finite-difference method using a semi-implicit Crank-Nicolson scheme (see the Appendix), with the boundary conditions $h_x=h_{xxx}=0$ on both ends of the computational interval. Figure 2 shows the film profiles for different values of the parameters. The propagating front develops a bump, better seen in the enlarged inset. When the evaporation rate is large [Fig. 2(a)], the bump gradually decreases, so that the final stationary profile becomes monotonic. At lower evaporation rates [Fig. 2(b)], the bump persists.

The solutions shown in Figs. 2(a) and 2(b) represent the fronts between the two equilibrium states propagating with

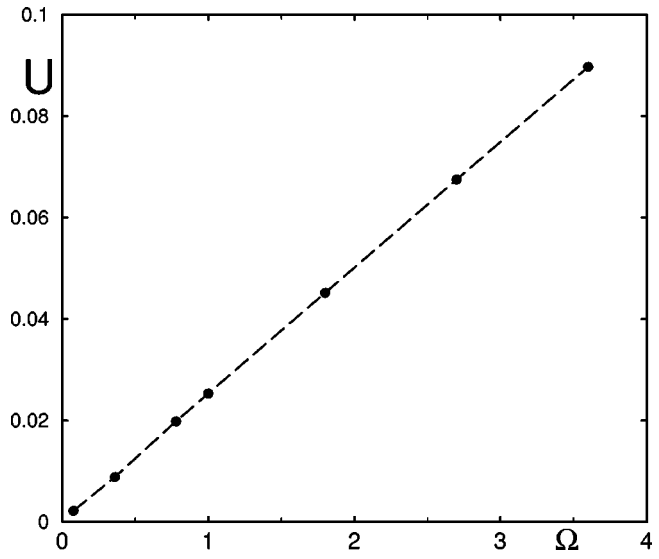

FIG. 3. Dependence of the front propagation speed U on the evaporation parameter Ω for $M=-0.003$, $\chi=1.085$.

constant speeds, which can be obtained from the computation data either directly (by tracking the motion of the profile) or by using the analytical formula

$$U=\frac{\Omega}{h_2-h_1}\int_{-\infty}^{\infty}\left(-\frac{1}{h^3}+e^{-\chi h}\right)dx, \tag{6}$$

where $h(x)$ is a numerically computed stationary profile. Both methods were implemented to check that identical results were obtained. The dependence of the front propagation speed U on the dimensionless parameter Ω characterizing the evaporation rate is shown in Fig. 3.

The dependence is almost linear, which means that the computation using Eq. (6) is only very slightly affected by changes of the film profile with changing Ω. Note that the equilibrium thickness does not depend on Ω. For $\Omega\to 0$, the propagation speed of a single one-dimensional front vanishes due to mass conservation.

IV. FINGERING INSTABILITY OF MOVING FRONTS

A. Linear analysis

In order to study the linear stability of a moving front between the ''dry'' and the ''wet'' regions of the film, obtained numerically in the form of a stationary wave solution $h_0(\xi)$, $\xi=x-Ut$, in the preceding section, consider infinitesimal perturbations of the front, $\tilde{h}=u(\xi)\exp(\omega t+iky)$, where ω is the growth rate and k is the spanwise wave number (along the y axis aligned with the front).

Linearization leads to the following eigenvalue problem:

$$\omega u+\mathcal{L}_0 u+k^2\mathcal{L}_2 u+k^4 h_0^3 u=0, \tag{7}$$

where the linear differential operators $\mathcal{L}_0$ and $\mathcal{L}_2$ are described in the Appendix. The eigenvalue problem has been solved numerically by discretizing Eq. (7) on the interval $[-L_1,L_2]$ and using homogeneous boundary conditions that

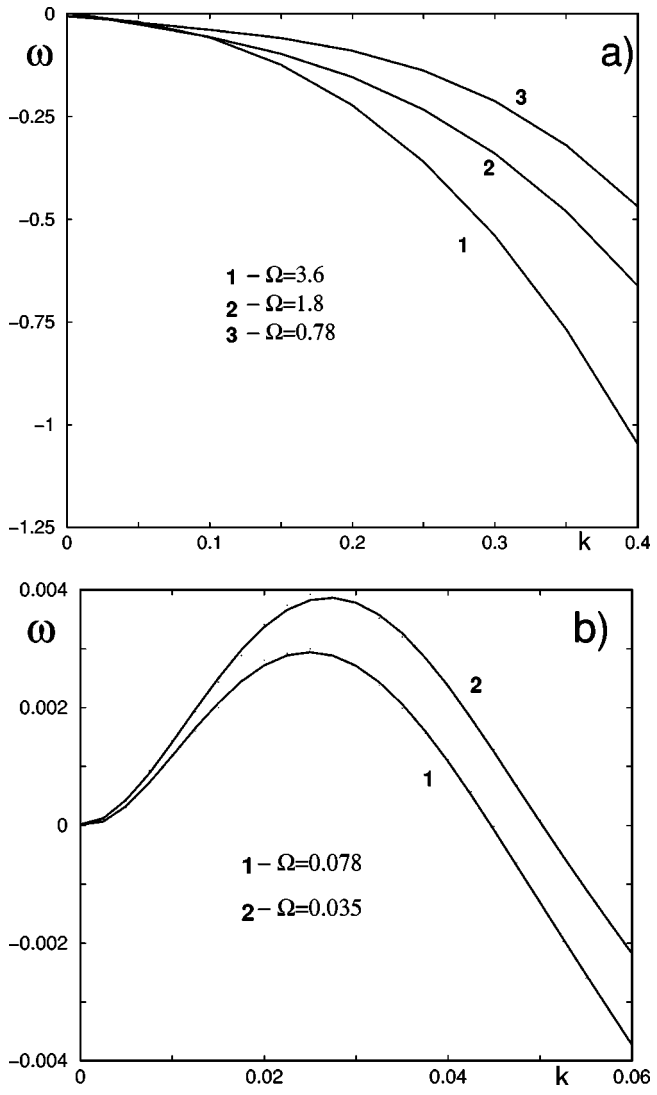

FIG. 4. Dispersion relations $\omega(k)$ for transversely stable (a) and unstable (b) propagating fronts for $M=-0.003$, $\chi=1.085$, and different values of Ω.

should be satisfied by the zero (Goldstone) mode $h_{0\xi}$ (see the Appendix). Numerical solution of this eigenvalue problem gives the dispersion relation $\omega(k)$. Some typical dispersion relations are shown in Fig. 4.

One can see that when the evaporation rate is high, all transverse perturbations decay. However, with the decrease of Ω, instability occurs with a nonzero wave number corresponding to the maximum growth rate [Fig. 4(b)]. This type of instability corresponds to fingering patterns observed in experiments with drying thin liquid films [7–9].

B. Instability threshold

The threshold of the transverse fingering instability corresponds to $k=0$, i.e., to the long-wave perturbations. In order to find the long-wave limit of the fingering instability of the moving fronts, consider Eq. (7) in the form

$$\omega u=\mathcal{L}u. \tag{8}$$

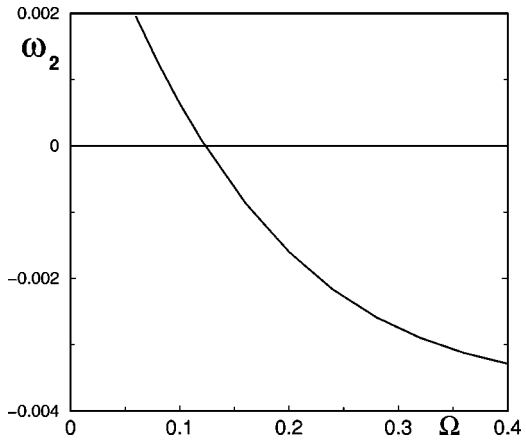

FIG. 5. The second-order coefficient in the dispersion relation ω_2 as a function of Ω for $M=-0.003$ and $\chi=1.085$.

For small wave numbers k, the perturbation growth rate is expanded as

$$\omega(k)=\omega_2 k^2+\omega_4 k^4+\cdots.$$

Expanding also

$$u=u_0+k^2u_2+\cdots, \quad \mathcal{L}=\mathcal{L}_0+k^2\mathcal{L}_2+\cdots,$$

one obtains from Eq. (7) the following eigenvalue problem for u_2:

$$\mathcal{L}_0u_2=-\omega_2u_0-\mathcal{L}_2u_0. \tag{9}$$

The solvability condition of this equation is

$$\omega_2=-\frac{\int_{-\infty}^{\infty}u_0^{\dagger}\mathcal{L}_2u_0dx}{\int_{-\infty}^{\infty}u_0u_0^{\dagger}dx}, \tag{10}$$

where u_0 is the Goldstone mode of the operator $\mathcal{L}_0$ and $u_0^{\dagger}$ is the corresponding eigenfunction of the operator adjoint to $\mathcal{L}_0$, given in the Appendix. The eigenfunction of the adjoint operator corresponding to the zero eigenvalue has been computed numerically and used in Eq. (10) to obtain ω_2 as a function of the evaporation parameter Ω. The result is shown in Fig. 5. The critical value of the parameter Ω corresponding to the onset of transverse instability is $\Omega_{cr}=0.121$ for $M=-0.003$, $\chi=1.085$.

C. Two-dimensional computations of the fingering instability

We have performed direct numerical simulations of Eq. (4) in two dimensions by means of the Crank-Nicolson finite-difference scheme. In order to solve the resulting nine-diagonal system of linear equations we have used the Stone algorithm [14] for sparse matrices. The computations have been performed on a grid 41×41 with the time step[2] $\Delta t=10^{-3}$. Figure 6 presents the film profiles for $\chi=1.085$, $M=-0.003$, and two different values of Ω. At high evaporation rates, the leading edge of the film remains stable [Fig. 6(a)]. At low evaporation rates, one can see the development of the fingering instability of a propagating front [Fig. 6(b)].

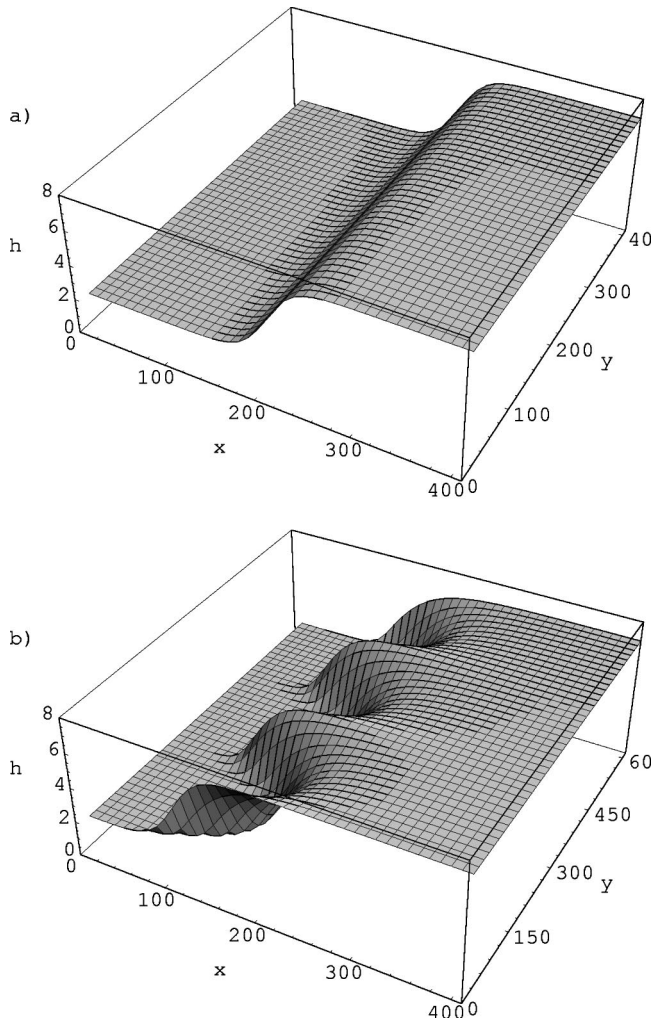

FIG. 6. Film shapes for $\chi=1.085$, $M=-0.003$, and $\Omega=0.78$ (a) and 0.078 (b).

V. EFFECT OF SUBSTRATE INHOMOGENEITIES ON THE FINGERING INSTABILITY OF DRYING FILMS

Substrate inhomogeneity is a very important factor which can substantially affect the dynamics of thin liquid films and their stability [15–17]. In order to model possible effects of the substrate inhomogeneity on the fingering instability of growing dry patches in a thin evaporating film of a polar liquid, we have considered the case when the Hamaker constant is a periodic function of the longitudinal coordinate. In this case, the motion of the front between two stable states of thin liquid film is described by Eq. (1) with $g(h)$ defined by Eq. (2) with the Hamaker constant being a periodic function

[2]In order to check the scheme accuracy the computations were also performed for the grids 81×81 and 101×101. The difference in the results was less than 2%.

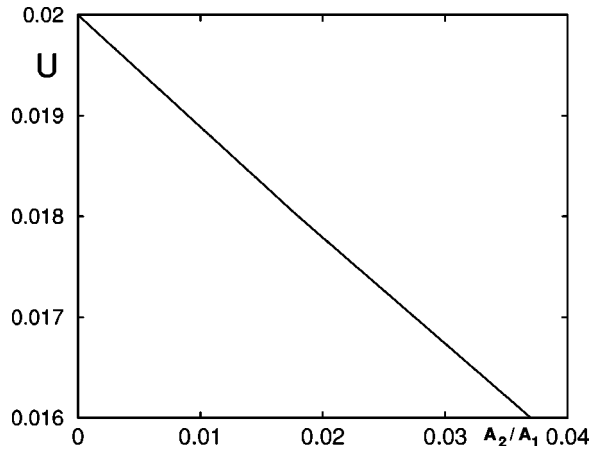

FIG. 7. The dependence of the front propagation speed on the relative amplitude of the inhomogeneity of the Hamaker constant.

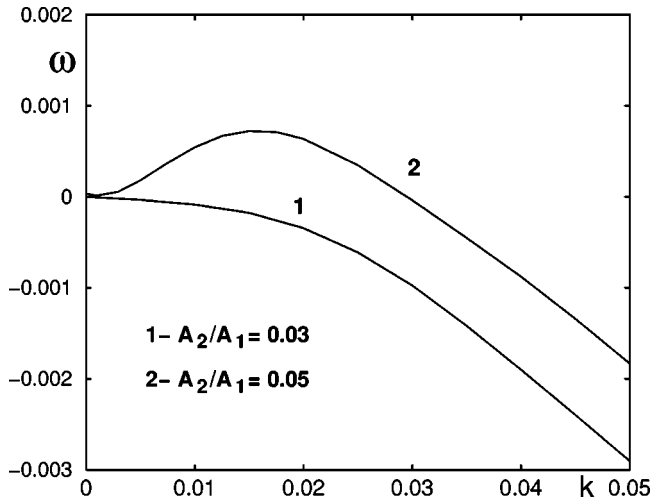

FIG. 8. Dispersion curves $\omega(k)$ corresponding to two different values of A_2/A_1 characterizing the surface inhomogeneity.

of the longitudinal coordinate x:

$$A = A_1 + A_2 \sin\frac{2\pi}{\lambda}x. \tag{11}$$

We considered only values of A_2 such that the variation of A does not change the number of stationary states of the evaporating liquid film corresponding to the given value of the vapor chemical potential μ_v (two stable and one unstable states). Due to this choice of the periodically varying Hamaker constant, the dimensionless parameters Ω and χ in Eq. (4) are also periodic functions of x:

$$\Omega = \Omega_0 + \Omega_1 \sin\frac{2\pi}{\lambda}x, \quad \chi = \chi_0 + \chi_1 \sin\frac{2\pi}{\lambda}x. \tag{12}$$

We have simulated Eq. (4) with Ω and χ given by Eq. (12) and found the effect of the surface inhomogeneity on the front propagation speed (i.e., the rate of the dry patch growth). The dependence $U(A_2/A_1)$ is shown in Fig. 7. One can see that the front speed (i.e., the growth rate of a dry patch) decreases with increase of the surface inhomogeneity amplitude. In accordance with the above conclusions on the effect of the front speed on its fingering instability, the surface inhomogeneity also leads to destabilization of the front. This is illustrated in Fig. 8 where two dispersion curves are presented, corresponding to two different values of the A_2/A_1 ratio.

VI. CONCLUSIONS

We have studied the fingering instability of growing dry patches in an evaporating film of a polar fluid. We have demonstrated that the mechanism of the instability is the same as that of the fingering instability in gravity or thermocapillary driven films, i.e., the formation of a ridge on the moving front between two states of the liquid film corresponding to two different thicknesses. The ridge formation is controlled by the front speed, which is proportional to the evaporation rate. An increase of the evaporation rate decreases the ridge and stabilizes the front. This situation is in contrast with the case of gravitationally or thermocapillary driven films where increasing front speed destabilizes the front.

For the parameter values typical of experiments carried out in [8,9] (see Sec. II) our computations predict the wavelength of the most unstable perturbation to be about 1 μm. This is in fair agreement with experimental observations [8,9], where a typical wavelength of the rim instability at the initial stage was found to be a few micrometers and the characteristic wavelength of the well-developed strongly nonlinear structure was found to be about 10 μm. It would be interesting to check experimentally our prediction about the dependence of the rim instability on the rate of the film evaporation. We are not aware of such measurements at present.

Our investigation of the influence of the substrate chemical heterogeneity on the fingering instability of growing dry patches reveals its retardation effect on the front speed, leading to enhancement of the fingering instability of the front.

ACKNOWLEDGMENTS

This work was supported by the Israel Science Foundation. The authors are grateful to Steven Lipson and Alex Oron for helpful discussions.

APPENDIX

The system of linear algebraic equations resulting from the semi-implicit Crank-Nicolson scheme of numerical solution of Eq. (4) on the $(n+1)$th time step is

$$A_j u_{j-2}^{n+1} + B_j u_{j-1}^{n+1} + C_j u_j^{n+1} + D_j u_{j+1}^{n+1} + E_j u_{j+2}^{n+1} = F_j^n, \tag{A1}$$

$$A_j = -\frac{\Delta t}{2(\Delta x)^3}\left[\frac{N_4}{\Delta x} - \frac{N_3}{2}\right],$$

$$B_j=\frac{\Delta t}{\Delta x}\left[\frac{2N_4}{(\Delta x)^3}-\frac{N_3}{2(\Delta x)^2}-\frac{N_2}{2\Delta x}+\frac{N_1}{4}\right],$$

$$C_j=\left[-\frac{3\Delta t}{(\Delta x)^4}N_4+\frac{\Delta t}{(\Delta x)^2}N_2+1-\frac{\Delta t}{2}N_0\right],$$

$$D_j=\frac{\Delta t}{\Delta x}\left[\frac{2N_4}{(\Delta x)^3}+\frac{N_3}{2(\Delta x)^2}-\frac{N_2}{2\Delta x}-\frac{N_1}{4}\right],$$

$$E_j=-\frac{\Delta t}{2(\Delta x)^3}\left[\frac{N_4}{\Delta x}+\frac{N_3}{2}\right],$$

where

$$N_4=-h^3,$$

$$N_3=-3h^2h_x,$$

$$N_2=\frac{3}{h}-\chi h^3\exp(-\chi h)+\Omega,$$

$$N_1=-3h^2h_{xxx}-2h_x\left[\frac{3}{h^2}+(3-\chi h)\chi h\exp(-\chi h)\right],$$

$$N_0=-3h^2h_{xxx}-6hh_xh_{xxx}+\left[-\frac{3}{h^2}-(3-\chi h)\times\chi h\exp(-\chi h)\right]h_{xx}-\left[-\frac{6}{h^3}+(6-6\chi h+\chi^2h^2)\times\chi h\exp(-\chi h)\right]h_x^2+\Omega\left[-\frac{3}{h^4}+\chi\exp(-\chi h)\right].$$

Here Δx and Δt are steps in space and time, respectively.

The linear differential operators in Eq. (7) are

$$\mathcal{L}_0=\frac{d}{dx}\left[f_{03}\frac{d^3}{dx^3}+f_{01}\frac{d}{dx}+f_{00}\right]+f_{000}, \tag{A2}$$

$$\mathcal{L}_2=f_{22}\frac{d^2}{dx^2}+f_{21}\frac{d}{dx}+f_{20}, \tag{A3}$$

where

$$f_{03}=h_0^3,\quad f_{01}=\frac{3}{h_0}-\chi h_0^3\exp(-\chi h_0)+\Omega,$$

$$f_{00}=U+h_{0x}\left[-\frac{3}{h_0^2}-(3-\chi h)\chi h^2\exp(-\chi h_0)\right]-3h_0^2h_{0xxx},$$

$$f_{000}=-\Omega\left[\frac{3}{h_0^4}-\chi\exp(-\chi h_0)\right],$$

$$f_{22}=2h_0^3,\quad f_{21}=3h_0^2h_{0x},\quad f_{20}=-f_{01}.$$

The boundary conditions for the problem (7) are

$$u_{-1}=\alpha_{11}u_1+\alpha_{10}u_0,\quad x=L_1,$$

$$u_{-2}=u_2+\beta_{11}u_{11}+\beta_{10}u_0=0,\quad x=L_1,$$

$$u_{N+1}=\alpha_{21}u_{N-1}+\alpha_{20}u_N,\quad x=L_2,$$

$$u_{N+2}=u_{N-2}+\beta_{21}u_{N-1}+\beta_{20}u_N=0,\quad x=L_2,$$

where

$$\alpha_{11}=-\frac{2+a_1\Delta t}{2-a_1\Delta t},\quad \alpha_{10}=\frac{b_1(\Delta t)^2-2}{1-a_1\Delta t/2},$$

$$\alpha_{21}=\frac{-2+a_2\Delta t}{2+a_2\Delta t},\quad \alpha_{20}=\frac{2-b_2(\Delta t)^2}{1+a_2\Delta t/2},$$

$$\beta_{11}=2(-1+\alpha_{11})+2a_1\Delta t(1+\alpha_{11})+b_1(\Delta t)^2(1-\alpha_{11}),$$

$$\beta_{10}=-4a_1\Delta t+\alpha_{10}[2+2a_1\Delta t-b_1(\Delta t)^2],$$

$$\beta_{21}=2(-1+\alpha_{21})-2a_2\Delta t(1+\alpha_{21})+b_2(\Delta t)^2(1-\alpha_{21}),$$

$$\beta_{20}=4a_2\Delta t+\alpha_{20}[2-2a_2\Delta t-b_2(\Delta t)^2],$$

$$a_1=-(\lambda_1+\lambda_2),\quad b_1=\lambda_1\lambda_2,$$

$$a_2=-2\,\mathrm{Re}(\lambda_3),\quad b_2=|\lambda_3|^2,$$

where λ_i are the roots of the characteristic equation of the linear problem with $k=0$ and $h_0=h_{1,2}=\mathrm{const}$ corresponding to the boundary condition $\tilde{h}\to 0$ for $x\to\pm\infty$.

The linear operator adjoint to $\mathcal{L}_0$ in Eq. (7) can be found according to the procedure described in Ref. [6]. This yields

$$\mathcal{L}_0^+=h_0^3\frac{d^4}{dx^4}+9h_0^2h_{0x}\frac{d^3}{dx^3}+\left[9(h_0^2h_{0x})_x+h_0^3\left(\frac{3}{h_0^4}-\chi e^{-\chi h_0}\right)+\Omega\right]\frac{d^2}{dx^2}+[18h_0h_{0x}h_{0xx}+6h_{0x}^3+6h_{0xxx}h_0^2-U]\frac{d}{dx}+(4h_{0x}^2-2h_0h_{0xx}-hh_0^2\chi+2h_{0x}^2-h_0h_{0x}\chi)h_0^2\chi^2e^{-\chi h_0}-\Omega\left(\frac{3}{h_0^4}-\chi e^{-\chi h_0}\right). \tag{A4}$$

[1] A. M. Cazabat, F. Heslot, P. Carles, and S. M. Troian, Adv. Colloid Interface Sci. **39**, 61 (1992).

[2] D. E. Kataoka and S. M. Troian, J. Colloid Interface Sci. **192**, 350 (1997).

[3] D. E. Kataoka and S. M. Troian, J. Colloid Interface Sci. **203**, 335 (1998).

[4] A. L. Bertozzi and M. P. Brenner, Phys. Fluids **9**, 530 (1997).

[5] I. Veretennikov, A. Indeikina, and H.-C. Chang, J. Fluid Mech. **373**, 81 (1998).

[6] Y. Ye and H.-C. Chang, Phys. Fluids **11**, 2494 (1999).

[7] M. Elbaum and S. G. Lipson, Phys. Rev. Lett. **72**, 3562 (1994).
[8] N. Samid-Merzel, S. G. Lipson, and D. S. Tannhauser, Phys. Rev. E **57**, 2906 (1998).
[9] N. Samid-Merzel, S. G. Lipson, and D. S. Tannhauser, Physica A **257**, 413 (1998).
[10] G. Reiter, Langmuir **9**, 1344 (1993).
[11] V. S. Mitlin, J. Colloid Interface Sci. **156**, 491 (1993).
[12] A. Sharma, Langmuir **9**, 861 (1993).
[13] A. Oron, S. G. Bankoff, and S. H. Davis, Rev. Mod. Phys. **69**, 931 (1997).
[14] H. L. Stone, SIAM (Soc. Ind. Appl. Math.) J. Numer. Anal. **5**, 530 (1968).
[15] R. Konnur, K. Kargupta, and A. Sharma, Phys. Rev. Lett. **84**, 931 (2000).
[16] K. Kargupta, R. Konnur, and A. Sharma, Langmuir **17**, 1294 (2001).
[17] K. Kargupta and A. Sharma, Phys. Rev. Lett. **86**, 4536 (2001).